MICRO-INCLUSIONS AND LOADS EFFECT ON METAL FATIGUE: A MODIFIED LIFE ESTIMATION MODEL THROUGH EXPERIMENTAL AND ANALYTICAL INVESTIGATION

Proceedings IRF2020: 7th International Conference Integrity-Reliability-Failure.
J.F. Silva Gomes and S.A. Meguid (editors), INEGI-FEUP (2020), pp.297-308.
https://paginas.fe.up.pt/~irf/Proceedings_IRF2020/

PAPER REF: 17281

MICRO-INCLUSIONS AND LOADS EFFECT ON METAL FATIGUE: A MODIFIED LIFE ESTIMATION MODEL THROUGH EXPERIMENTAL AND ANALYTICAL INVESTIGATION

Raffaella Sesana[1(*)], Irene Pessolano Filos[1], Nicolas Oyarzabal[2], Andrea Uva[3]

[1]DIMEAS, Politecnico di Torino, Italy
[2]Instituto Tecnologico de Buenos Aires, Argentina
[3]Central Lab - Product Development, Tsubaki Nakashima, Italy
[(*)]*Email:* raffaella.sesana@polito.it

ABSTRACT

Fatigue life calculation of a metal component accounts for different phenomena. External factors, such as load type, as well as internal microstructure, play a major role in determining fatigue failure. The present paper explores the relationship between micro-inclusions in hard steels and fatigue behaviour. Tension- compression and rotating bending tests were performed on two steel alloys with different grades. Micro- inclusions presence and characteristics are quantified by a non- destructive SEM technique. The stress field around micro- inclusions is quantified by Eshelby's model. A microstructural study is applied to relate failure and micro-inclusion parameters. This approach leads to the identification of a modified life model and stress intensity factor in the two loading cases.

Keywords: tensile- compression test, rotating bending test, micro- inclusions, 100Cr6, Eshelby's method, stress intensity factor.

INTRODUCTION

The surface of solids presents defects and distortions. Surface imperfections exert a strong influence on friction and wear [1]. The contact or surface fatigue is the term used to identify the surface damage prompted by repeated rolling contact between asperities, high local stresses and wear particles. Those phenomena induce fatigue cracks propagation [2].

RCF is the acronym to identify the rolling contact fatigue, the most common damage cause in mechanical components involving rolling or sliding contact such as balls or roller bearings, gears, cams, railways. Systems undergoing structural fatigue (SF) and RCF are subjected to material failure due to the application of repeated stresses in a small volume (typical bearing contact widths are in the order of 200-1000 μm [3]). SF can be often modelled as an equivalent uniaxial and usually tensile phenomenon, while RCF generates a multiaxial state of stress which makes the estimation of component life complex. The most descriptive nomenclature of the physical evaluation of each damage mechanism is the one proposed and used by [4]. It is well known that roughness is the main cause of crack initiation in RCF of hard steel components [4] and generally in fatigue crack nucleation. The typical depth of micropitting is approximately 10 μm. If the microcrack reaches the critical size, there is material detachment and consequently the micropitting takes place. The depth of the detached fragment has a typical dimension of 10 μm [5]. Authors of reference [5] propose a stress index $\Delta\tau$ for cyclic shear stresses at the critical plane. The formation of the so called "butterflies" leads to cracks at porosity or at small non-

metallic inclusions. They are the first signs of subsurface damage in high strength steels [5]. Reference [6] analysed from a microstructural point of view the "butterflies" in standard 100Cr6 bearing steel and focused the study on iron beam tomography to reveal voids presence, then transmission electron microscopy to reveal superfine nano- grains. Spalling is favoured by factors such as smooth surfaces, presence of non- metallic inclusions in material and absence of surface shear. Due to those factors, below the surface microcraks generation, propagation towards the surface and spall formation occur [3]. Also in this case, it is defined a damage index as the maximum ratio between shear stress and local hardness for case hardening with hardness gradient [7]. Their experiments showed that subsurface damage initiated for the highest ratio and in case of a group of cracks and not only a single crack.

The relation between the fatigue resistance of a material with and without microinclusion is deeply investigated by [26] [27] who adapted the original Peterson approach, which was proposed for large notches, to small cracks, small defects and nonmetallic inclusions.

Reference [8] evaluated with FEM calculations the propagation index as the ratio of applied and threshold stress intensity factors. Then, Murakami approach [9] was used to find the link between material hardness and inclusion size.

Fatigue wear control acts on physical parameters such as applied stress level, operating temperature, number of revolutions, material parameters, heat treatments, residual stress level [3]. Over the last decade significant bearing performance increase was reached also due to cleanliness improvement [10]. Steelmaking process is affected by variation and inhomogeneity in the composition of ferroalloys. Reference [10] analyses the main factors influencing steel cleanliness through ferroalloy addition: inclusion, available oxygen and sulphur, amount of base metal and elemental impurities in the ferroalloy. Non-metallic inclusions are chemical compounds and non-metals in steels and alloys. They cannot be eliminated in the steelmaking process given that they are the products of chemical reactions, physical effect, and contamination during melting and pouring processes. Four macro-categories, sulphides, aluminates, silicates and oxides, are identified to classify non-metallic inclusion by ASTM E45 – 18A Standard [11].

The steel alloys quality indicators rely on Standards (such as in references [11] or [24]) suggesting metallographic methods linking the steel cleanliness assessment to the micro-inclusion population. I.g., Extreme Value Analysis (EVA) is used by [12] and [13]. Offline steel cleanliness determination methods and online techniques are used to study steel refining and casting issues. At all stages in steel production, the amount, size distribution, shape and composition of inclusions should be measured [14]. Direct inspection methods for inclusion evaluation of solid steel section, such as Metallographic Microscope Observation (MMO), Image Analysis (IA) or Scanning Electron Microscopy (SEM) are accurate but costly. On the other side, indirect methods, such as Conventional Ultrasonic Scanning (CUS) or Mannesmann Inclusion Detection by Analysis Surf-boards (MIDAS) are fast and low cost [14].

Inclusions act as a stress raiser and factors such as dimension, depth, shape, and chemical composition affect the stress peak. The characterization of steel cleanliness is evaluated by the total oxygen content. It is the sum of the soluble oxygen in liquid steel (oxide inclusions) [16]. In reference [17] the proposed model analyses the life reduction correlated to size, shape, orientation, location of microinclusions and stress alterations to steel bearing material in case of inclusions presence. Ai *et al.* [17], in his study, links the inclusion length with the stressed volume under contact load by a regression equation for predicting the bearing life reduction factor (LRF).

In the bearing market, 100Cr6 is largely used. For this reason, it is also employed for a research point of view. Kang *et al.* [12] used a 100Cr6 in ball on rod RCF tests, and investigated the inclusions effect on fatigue failure: the stress concentration around inclusions leads to microcracks formation.

The experimental results described in reference [13] focused on endurance limit. It is higher in case of cleaner steel for equal hardness and heat treatment. Wear resistance has been largely studied over the years. Authors of reference [18] considered the cryogenic treatment to enhance it on 100Cr6 bearing steel. Those procedures, compared to conventional heat treatment, produce more martensite transformation (reducing the retained austenite amount) and carbide formation, thus tougher grains and higher wear resistance.

Ultrasonic high frequency echography was also used to investigate subsurface damage in [19] study. This technique could precisely locate cracks and permit to determine depth and angular orientation. The aim of [19] is to experimentally obtain the correlation between failure and inclusions for different steels composition and loading conditions.

The aim of the present research is to investigate the effect of micro-inclusions in hard steels on fatigue behaviour in different loading conditions, that is, rotating bending and axial tension-tension testing.

ANALYTICAL BACKGROUND

Understanding the mechanisms of fatigue and machinability of steels is the basis to quantitatively evaluate the effect of defects from a practical engineering point of view [20][21]. Several techniques have been developed to consider defects, inclusion and inhomogeneities effects in fatigue strength. Murakami and Endo classified the models for fatigue limit stress evaluation of metals in the presence of small defects [22]. There are three main types of existing models used to identify fatigue strength. Frost's approach linked the fatigue limit with the crack length [23]. In the case of small defects, Murakami and Endo proposed the projection area of defects in [24]. Kitigawa and Takahashi pursued a fracture mechanics approach based on the intrinsic threshold stress intensity factor ΔKi_th; while Mitchell and Nordberg based their approach on fatigue notch factor.

Starting from Peterson's equation and classical fatigue approach, the fatigue resistance in presence of notches and taking into account of load effect is expressed by Marin equation [30]:

$$\sigma_w = \sigma_{w0} \frac{C_l}{K_f} \tag{1}$$

Where σ_{wo} is the fatigue strength of the material, σ_w the fatigue strength of the "defected" material, K_f is the fatigue stress concentration factor, C_l the so-called load factor, taking into account of the different testing conditions. According to reference [31], this last factor can be assumed 1 for rotating bending testing and 0,7 for axial fatigue testing.

According to reference [25], the notch sensitivity q is defined as:

$$q = \frac{K_f - 1}{K_t - 1} \tag{2}$$

where K_t is the stress intensity factor, defined on geometric parametric properties of notches.

In case of microinclusions and very small defects, according to reference [22], the same notch sensitivity is:

$$q = \frac{1}{1 + \frac{C'}{\varrho}} \tag{3}$$

where ϱ is the radius of the notch root and C' is a characteristic material parameter, which is a function of material UTS or HB [22]:

$$C' = 0.02534\left(\frac{600}{HB}\right)^{1,8} \; or \; C' = 0.02534\left(\frac{2070}{UTS}\right)^{1,8} \tag{4}$$

Then for small crack [22] the fatigue strength σ_w, in the case of a specimen with microinclusions, is:

$$\sigma_w = \frac{\sigma_{w0}}{1 + (K_t - 1)/\left(1 + \frac{C'}{\varrho}\right)} \tag{5}$$

where σ_{w0} is the fatigue strength of the microinclusion-free specimens.

Based on geometric and compositional data on microinclusions found at fatigue crack nucleation site, the stress intensity factor of the microinclusion can be calculated; and, based on experimental data obtained from fatigue testing campaigns of specimens with microinclusions, the fatigue limit of the material without microinclusions can be estimated.

MATERIALS AND METHODS

In the current investigation, a total of four samples of steel specimens were analysed. Sample one (S1) was 100Cr6 and sample 2 (S2) was 100CrSiMn 6-5-4. They were tested using the rotating bending method according to Standards ISO 1143 [26]. Rotating bending specimens design is such that the maximum stress occurs at midpoint. This avoids unwanted stress concentrations. Sample 3 (S3) was Grade A NiTi 4,5 mm thick and 45 mm2 sectional areas. Sample 4 (S4) was Grade B NiTiVMo 8 mm thick and 128 mm2 sectional area. S3 and S4 were subjected to axial fatigue tests. Tension- tension specimens were exposed to pure axial loading. The samples were shaped and tests were performed according to ASTM E466 [27]. The specimen is clamped at two ends and loaded cyclically between two extreme values (maximum and minimum). In both S4 and S3 tests, the fatigue stress ratio R was 0,1.

The following Table 1 and Table 2 summarize the chemical composition of the investigated samples.

Table 1 - Chemical composition 100Cr6 and 100CrSiMn6-5-4

100Cr6	**Element %**	**C%** 0.97	**Si%** 0.23	**Mn%** 0.29	**Ni%** 0.08	**Cr%** 1.43	**Mo%** 0.013	**Cu%** 0.05	**S%** 0.003
	Element %	**P%** 0.014	**Al%** 0.025	**As%** <0.01	**Sn%** <0.01	**Sb%** 0.002	**Pb%** 0.001	**Ti%** 0.001	**Ca%** <0.001
100CrSi Mn6-5-4	**Element %**	**C%** 1.03	**Si%** 1.20	**Mn%** 0.97	**Ni%** 0.12	**Cr%** 1.47	**Mo%** 0.04	**Cu%** 0.13	**S%** 0.005
	Element %	**P%** 0.013	**Al%** 0.02	**As%** 0.01	**Sn%** 0.01	**Sb%** 0.001	**Pb%** 0.003	**Ti%** <0.001	**Ca%** <0.0005

Table 2 - Chemical composition Grade A and Grade B

Element	**C %**	**Mn + Si %**	**P %**	**S %**	**Mo %**	**Al %**	**N (ppm)**	**Nb %**	**Ti %**	**V %**
Max	0,1	2	0,1	0,01	0,04	0,1	100	0,1	0,5	0,1
Element	**C %**	**Mn + Si %**	**P %**	**S %**	**Mo %**	**Al %**	**N (ppm)**	**Nb %**	**Ti %**	**V %**
Max	0,1	2	0,02	0,005	0,6	0,1	100	0,05	0,05	0,1

The experimental set up consisted of a rotating bending machine mod. RB35 for sample S1 and S2. The bending moment applied to the central section of the specimen is constant. As the specimen rotates, the load acting on specimen induces a fluctuating bending stress. For each test type two campaigns (RB1 and RB2) were performed for 100Cr6 and 100CrSiMn6-5-4 respectively. For rotating bending experiments a set of 15 samples were tested. In the present paper, a Staircase [28] fatigue campaign was run at 3500 rpm, life target $5*10^6$ cycles and stress increment in Staircase testing $\Delta\sigma$=25MPa.

The axial fatigue testing machine INSTRON 8801 was used for samples S3 and S4. In this experiment, the specimen is exposed to pure axial (tensile or compressive) loading, with constant mean stress. For tension- tension tests, 21 specimens for the first campaign AF1 (Grade A) were tested and 22 for the second one AF2 (Grade B).

Table 3 compares the test characteristics in campaign 1 and 2 for RB1 and RB2 rotating bending experiments and AF3 and AF4 axial fatigue respectively.

Table 3 - Test characteristics for campaign 1 and 2 (Rotating bending)

	Material	**Stress frequency [Hz]**	**Life target [Cycles]**	**Δσ [MPa]**
RB1	100Cr6	58,3	$5*10^6$	25
RB2	100CrSiMn6-5-4	58,3	$5*10^6$	25
				R
AF1	Grade A	15	$3*10^6$	0,1
AF2	Grade B	15	$3*10^6$	0,1

After-failure analyses consisted in optical inspection on the fracture surface using a microscope to investigate the crack nucleation origin. Cleanliness analysis [11] were run to characterize the size, distribution, number, and type of inclusion on a polished specimen surface. The minimum polished area of a specimen for the microscopic determination of inclusion content was 170 mm^2. The type of inclusions encountered, and the representative photomicrographs were characterized in a section area of raw material. The sample was divided into standard inspection areas S_0 of 0,5 mm^2 and examined to find non-metallic inclusions.

A scanning electron microscope (SEM) was employed to know the chemical composition and dimension of the inclusions.

A FEM simulation [23] allowed the implemention of Eshelby's model to calculate the maximum stresses at the microinclusion boundaries. The comparison between the nominal stress and the maximum equivalent stress for each microinclusion allowed estimating the stress intensity factor [25] k_t related to the microinclusion. Then, according to Neuber's model [25], the estimation of the notch factor is obtained and the fatigue limit of the material without microinclusion is obtained according to [26][27].

The purpose of the first two test campaigns on 100Cr6 and 100CrSiMn 6-5-4 was to establish the fatigue limit of the material in rotating bending testing conditions. Table 4 and Table 5 summarize the results obtained from RB1 and RB2.

Table 4 - Campaign RB1 – Staircase 100Cr6

Test	Stress applied to A_{min}	Failed (F) Survived (S)	Cycles [10^6]	Test duration [h]
1	1100	F	1.24	5.9
2	1075	F	4.20	20.0
3	1050	F	1.06	5.1
4	1025	S	5.00	23.8
5	1050	F	3.11	14.8
6	1025	S	5.00	23.8
7	1050	S	5.00	23.8
8	1075	S	5.00	23.8
9	1100	F	4.00	19.0
10	1075	S	5.00	23.8
11	1100	S	5.00	23.8
12	1125	S	5.00	23.8
13	1150	F	1.73	8.2
14	1125	S	5.00	23.8
15	1150	S	5.00	23.8

Table 5 - Campaign RB2 – Staircase 100CrSiMn6-5-4

Test	Stress applied to A_{min}	Failed (F) Survived (S)	Cycles [10^6]	Test duration [h]
1	1025	F	0.24	1.1
2	1000	S	5.00	23.8
3	1025	F	0.30	1.4
4	1000	F	0.05	0.3
5	975	S	5.00	23.8
6	1000	F	1.56	7.4
7	975	F	0.01	0.1
8	950	F	1.48	7
9	925	S	5.00	23.8
10	950	F	1.92	9.1
11	925	F	0.44	2.1
12	900	S	5.00	23.8
13	925	S	5.00	23.8
14	950	S	5.00	23.8
15	975	S	5.00	23.8

Tensile tests were performed to obtain the Wholer curve and the fatigue limit for specimens Grade A and B. Table 6 and Table 7 summarize the results obtained from the two campaigns. Table 8 provides the fatigue resistance experimental values for the different samples and different loaded conditions. For AF1 and AF2 specimens, which were tested with R=0,1, the fatigue resistance σ^*_{D-1}, corresponding to R=-1, was extrapolated by means of Goodman equation.

Table 6 - Campaign AF1: S-N Grade A

Test	σ_{max} [MPa]	σ_{min} [MPa]	σ_a [MPa]	Cycles to Failure [10^6]	F/S
1	609.7	60.97	274.37	0.04	F
2	609.7	60.97	274.37	0.06	F
3	583.2	58.32	262.44	0.40	F
4	524.9	52.49	236.21	0.11	F
5	524.9	52.49	236.21	0.17	F
6	524.9	52.49	236.21	0.19	F
7	514.3	51.43	231.44	0.25	F
8	514.3	51.43	231.44	0.27	F
9	514.3	51.43	231.44	0.34	F
10	498.4	49.84	224.28	0.31	F
11	498.4	49.84	224.28	0.36	F
12	498.4	49.84	224.28	0.43	F
13	498.4	49.84	224.28	3.00	S
14	487.8	48.78	219.51	0.55	F
15	487.8	48.78	219.51	0.58	F
16	487.8	48.78	219.51	0.64	F
17	477.2	47.72	214.74	0.48	F
18	477.2	47.72	214.74	0.76	F
19	477.2	47.72	214.74	2.06	F
20	466.5	46.65	209.93	3.00	S
21	466.5	46.65	209.93	3.00	S
22	466.5	46.65	209.93	3.00	S

Table 7 - Campaign AF2: S-N Grade B

Test	σ_{max} [MPa]	σ_{min} [MPa]	σ_a [MPa]	Cycles to Failure [10^6]	F/S
1	608.4	60.84	273.78	0.1	F
2	608.4	60.84	273.78	0.14	F
3	608.4	60.84	273.78	0.21	F
4	597.1	59.71	268.70	0.17	F
5	597.1	59.71	268.70	0.18	F
6	597.1	59.71	268.70	0.21	F
7	585.9	58.59	263.66	0.2	F
8	585.9	58.59	263.66	0.2	F
9	585.9	58.59	263.66	0.21	F
10	574.6	57.46	258.57	0.28	F
11	574.6	57.46	258.57	0.31	F
12	574.6	57.46	258.57	0.65	F
13	563.3	56.33	253.49	0.38	F
14	563.3	56.33	253.49	0.42	F
15	563.3	56.33	253.49	3	S
16	552.1	55.21	248.45	0.22	F
17	552.1	55.21	248.45	0.48	F
18	552.1	55.21	248.45	3	S
19	540.8	54.08	243.36	3	S
20	540.8	54.08	243.36	3	S
21	540.8	54.08	243.36	3	S

Table 8 - Fatigue resistance σ^*_{D-1} experimental values

Campaign	Material	Fatigue limit [MPa]	Campaign	Material	Fatigue limit [MPa]
RB1	100Cr6	1075 ± 32.2	**AF1**	Grade A	357
RB2	100CrSiMn6-5-4	927.5 ± 22.3	**AF2**	Grade B	432

Optical inspections were performed on failed specimens and they showed that in all the specimens the fracture starting point was an inclusion just below the external surface. As an example, in Figure 1 two microscopic views related to one specimen of each sample of RB campaigns are shown.

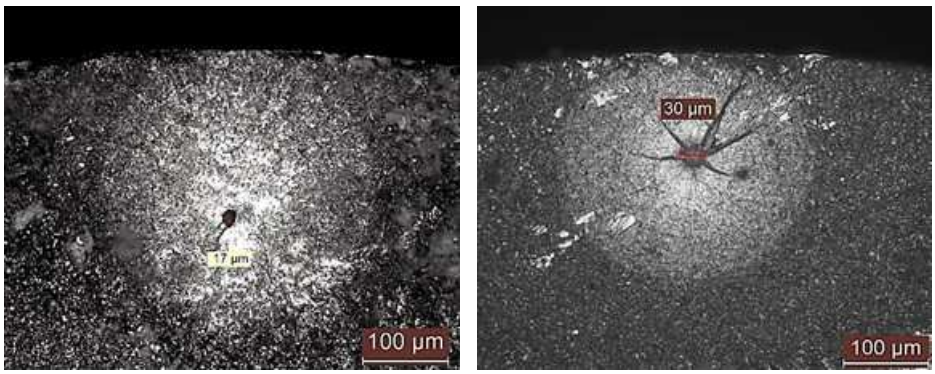

Fig. 1 - specimens fracture surface, crack nucleation points: S1 (left) and S2 (right)

Aluminum oxides Al_2O_3 and others (e.g.: calcium aluminate) are the initiator of fracture. Table 9 reports the results of stress calculations according to De Saint Venant theory and Eshelby's model at microinclusion boundaries for failed specimens for the different samples. In columns 4, 5 and 6 inclusion dimensions along the three axes of global reference system and in column 7 the depth with respect to sample surface at which the microinclusion is positioned are reported. Moreover, the maximum equivalent Tresca stress σ_{nT} in the same position (assuming no microinclusion is present) and maximum equivalent Tresca stress σ_{iT} calculated employing Eshelby's model and numerical simulation (corresponding to the presence of the microinclusion), the percent difference σ_{inc} between σ_{iT} and σ_{nT}, the actual life of specimens with microinclusions are summarized in column 8-11 [29]. For what concerns microinclusion composition, when different compositions were found in the same fracture surface, the stiffest one's Young modulus and the Poisson ratio were assumed in the calculations.

Previous studies on samples subjected to rotating bending tests have shown a higher percentage of Silicon on 100CrSiMn 6-5-4 steel and data from several sources have identified the increase in fatigue limit associated with the Silicon (Si) [20] and Molybdenum (Mo) content [21][22].

Contrary to the expectations, the present test results showed that the fatigue limit of 100CrSiMn6-5-4 is lower than that of 100Cr6. This result may be explained by the fact that after failure analysis showed more critical inclusions in 100CrSiMn6-5-4 than 100Cr6. Consequently, fatigue limit is reduced.

Table 9 - Inclusion composition, geometry, position and equivalent stresses calculation

Test		composition	Inclusion dimension			inclusion depth	σ_{nT} [MPa]	σ_{iT} [MPa]	σ_{inc} [%]	Cycles to failure
			x	y	z					
S1, S2	5	Al_2O_3	12,5	12,5	12,5	-54	1025	1268	24	3110000
	9	Al_2O_3	9,5	9,5	9,5	-126	1038	1284	24	4000000
	3	Al_2O_3	23,5	23,5	23,5	-100	979	1211	24	300000
	11	Al_2O_3	31	31	31	-227	832	1134	36	440000

The previous investigation on samples employed in tensile- tensile tests has found a higher percentage of Molybdenum (Mo) in Grade B. Moreover, a higher Molybdenum (Mo) content increases the fatigue limit [20], [21]. This study confirms the expectations and it is consistent

with the literature. Differently to the rotating bending tests, no critical inclusions have been identified as the starting point.

The correlation between fatigue and the presence of non-metallic inclusions for a different number of cycles was evaluated through SEM analysis on test 4, 9, 14, 17 and 19 for Grade A and on test 1, 5, 7, 11 and 13 for Grade B. No critical inclusions were found, nevertheless, flakes of non- metallic materials were found near the fracture starting points. This can mean that microinclusions were lost while fracture took place or they were not present. These results, therefore, need to be interpreted with caution: it is impossible to say that these inhomogeneities are the cause of the failure but they may have contributed to increase the stress and leading to crack. Since no inclusions were found near the starting points, cleanliness analysis was performed on a section of tension-tension specimens in order to verify the low contents of critical inclusions. An inspectional area of 14.5 cm^2 was analysed both in Grade A and B. Critical inclusions found are shown in Figure 2. Inclusion are defined critical when their evaluation is closed to the tolerance limit for the steel grade adopted for the RCF part in the bearing application. Other inclusions were found but not reported since they are small. Results showed that both grade A and grade B have low contents of critical inclusions as expected. Also, in these tests each specimen was manually sanded to reduce surface roughness from the abrasive waterjet cut. The final roughness was measured with a Mitutoyo SJ210 Tester and values between 0,03 and 0,2 μm were obtained for both samples. This difference in roughness could have influenced the number of cycles to failure for each one.

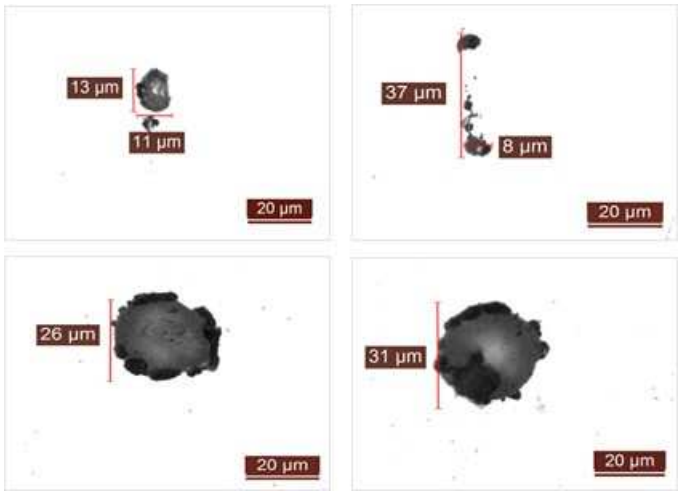

Fig. 2 - Oxides type - 1000x. Grade A (top) and Grade B (down)

For what concerns the life estimation, in Table 10 the summary of factor estimation is reported for the different material samples. The calculations were performed for an average microinclusion dimension.

The results in Table 10 are related to the microinclusion which leads the material to failure. Considering the fatigue failures, the material with higher mechanical properties failed for inclusions with wider radiuses, while the material with lower properties resulted to be sensitive to smaller radiuses of inclusions. This is coherent with experimental fatigue research and models for which the radius of curvature of the inclusion influences on the notch effect by means of the notch sensitivity q which is related, in both theories, to notch radius.

It can also be observed that the calculated notch sensitivity q differs for the two sets of materials in an order of magnitude, according to the same variation in the microinclusion curvature radius.

Table 10 - Estimation of microinclusion notch factor and of fatigue limit without microinclusions

	100Cr6	100CrSiMn6-5-4	Grade A	Grade B
Nominal stress [MPa] σ_{nT}	1025	979	236	268.7
Maximum stress at microinclusion boundaries [MPa] σ_{iT}	1268	1211	292	393
Stress intensity factor k_t	1.24	1.24	1.24	1.46
Experimental fatigue resistance [MPa] σ^*_{D-1}	1075	937	357	432
UTS [MPa]			623	679
HB	657	680		
C'	0.022	0.020	0.22	0.19
Microinclusion curvature radius [mm] φ	0.0125	0.0235	0.005	0.008
Notch sensitivity q	0.37	0.54	0.02	0.04
Load factor C_l	0.97	0.97	0.70	0.70
σ^*_{D-1}				
Fatigue notch factor k_f	1.09	1.13	1.01	1.02
Estimated fatigue resistance without inclusions [MPa] σ_{D-1}	1170	1054	513	629

Observing the calculated static stress intensity factor k_t, obtained by means of the ratio between Eshelby maximum stress σ_{iT} at the microinclusion boundary and the nominal stress σ_{nT}, this difference is less relevant. This may be due to the fact that the Eshelby's model is strongly dependent on material's mechanical properties and is related to all the geometric properties of the microinclusion, not only the curvature radius.

Considering the fatigue notch factor, assuming the Neuber and Peterson classical approach, corrected for the microinclusion with Murakami equations, it can be observed that the values for the two sets of material is not elevated, thus meaning that the combination of geometry and material properties is well taken into account by the microinclusion notch effect model. The estimation of the fatigue limit without microinclusion can contribute to evaluate the possible advantages deriving from controlling the alloy manufacturing process.

CONCLUSIONS

The aim of the investiagtion was to evaluate the effect of inclusions on material fatigue life prediction in different loading conditions.

Different tests on different steel composition and a numerical simulation were made in order to better understand the influence of inclusions on the fatigue life.

Two different raw materials under two different loading conditions were evaluated: 100Cr6 and 100CrSiMn6-5-4 were tested on rotating bending machine and Grade A and B on tension-tension machine.

Numerical simulation of Eshelby's model enabled to evaluate the increase of stress at the boundary of the inclusion for different shape, chemical composition and dimension.

Tests results have shown that the presence of inclusions has a primary importance on fatigue life, since, contrary to the expectation, the fatigue limit of the steel with more alloy elements was lower. Cleanliness analysis showed that higher alloy steel has more critical inclusions which counteract the positive effect on fatigue life of silicon and other alloy elements.

After defining the characteristics of inclusions, Eshelby's model was applied in order to calculate the corresponding stress peak at the boundary of the inhomogeneties.

From the calculated stress it is possible to evaluate the inclusion theoretical load that would produce the same stress nominal in absence of inclusions.

The microinclusion notch effect on static and fatigue loading was then estimated by means of Eshelby's model and Murakami approach. The estimated material fatigue resistance without microinclusions was finally estimated. The estimation of the fatigue limit without microinclusion can contribute to evaluate the possible advantages deriving from controlling the alloy manufacturing process.

REFERENCES

[1] Stachowiak GW, Batchelor AW, "Engineering Tribology - Fundamentals of contact between solids," 1993, p. 871.

[2] Stachowiak GW, Batchelor AW, "Engineering Tribology - Fatigue wear," in Engineering Tribology, 1993, p. 871.

[3] Moghaddam SM, Sadeghi F, "A Review of Microstructural Alterations around Nonmetallic Inclusions in Bearing Steel during Rolling Contact Fatigue," Tribol. Trans., vol. 59, no. 6, pp.1142-1156, 2016, doi: 10.1080/10402004.2016.1141447.

[4] Olver AV, "The mechanism of rolling contact fatigue: An update," Proc. Inst. Mech. Eng. Part J J. Eng. Tribol., vol. 219, no. 5, pp.313-330, 2005, doi: 10.1243/135065005X9808.

[5] Santus C, Beghini M, Bartilotta I, Facchini M, "Surface and subsurface rolling contact fatigue characteristic depths and proposal of stress indexes," Int. J. Fatigue, vol. 45, pp.71-81, 2012, doi: 10.1016/j.ijfatigue.2012.06.012.

[6] Evans MH, Walker JC, Ma C, Wang L, Wood RJK, "A FIB/TEM study of butterfly crack formation and white etching area (WEA) microstructural changes under rolling contact fatigue in 100Cr6 bearing steel," Mater. Sci. Eng. A, vol. 570, pp.127-134, 2013, doi: 10.1016/j.msea.2013.02.004.

[7] Leng X, Chen Q, Shao E, "Initiation and propagation of case crushing cracks in rolling contact fatigue," Wear, vol. 122, no. 1, pp.33-43, 1988, doi: 10.1016/0043-1648(88)90004-X.

[8] Bormetti E, Donzella G, Mazzù A, "Surface and subsurface cracks in rolling contact fatigue of hardened components," Tribol. Trans., vol. 45, no. 3, pp.274-283, 2002, doi: 10.1080/10402000208982550.

[9] Beswick JM, Bearing Steel Technology. 100 Barr Harbor Drive, PO Box C700, West Conshohocken, PA 19428-2959: ASTM International, 2002.

[10] Pande MM *et al.*, "Ferroalloy quality and steel cleanliness," Ironmak. Steelmak., vol. 37, no. 7, pp.502-511, 2010, doi: 10.1179/030192310X12700328925787.

[11] "Standard Test Methods for Determining the Inclusion Content of Steel 1," pp.1-20, 2005, doi: 10.1520/E0045-18A.1.7.

[12] Kang JH, Vegter RH, Rivera-Díaz-del-Castillo PAJ, "Rolling contact fatigue in martensitic 100Cr6: Subsurface hardening and crack formation," Mater. Sci. Eng. A, vol. 607, pp.328-333, 2014, doi: 10.1016/j.msea.2014.03.143.

[13] Oezel M, Janitzky T, Beiss P, Broeckmann C, "Influence of steel cleanliness and heat treatment conditions on rolling contact fatigue of 100Cr6," Wear, vol. 430–431, no. April, pp.272-279, Jul. 2019, doi: 10.1016/j.wear.2019.04.026.

[14] Zhang L, Thomas BG, "State of the Art in Evaluation and Control of Steel Cleanliness.," ISIJ Int., vol. 43, no. 3, pp.271-291, 2003, doi: 10.2355/isijinternational.43.271.

[15] Steneholm K, Andersson NAI, Tilliander A, Jönsson PG, "The role of process control on the steel cleanliness," Ironmak. Steelmak., vol. 45, no. 2, pp.114-124, 2018, doi: 10.1080/03019233.2016.1245917.

[16] Bartosiaki BG, Pereira JAM, Bielefeldt WV, Vilela ACF, "Assessment of inclusion analysis via manual and automated SEM and total oxygen content of steel," J. Mater. Res. Technol., vol. 4, no. 3, pp.235-240, Jul. 2015, doi: 10.1016/j.jmrt.2015.01.008.

[17] Ai X, "A Comprehensive Model for Assessing the Impact of Steel Cleanliness on Bearing Performance," J. Tribol., vol. 137, no. 1, pp.1-10, Jan. 2015, doi: 10.1115/1.4028467.

[18] Sri Siva R, Arockia Jaswin M, Mohan Lal D, "Enhancing the Wear Resistance of 100Cr6 Bearing Steel Using Cryogenic Treatment," Tribol. Trans., vol. 55, no. 3, pp.387-393, 2012, doi: 10.1080/10402004.2012.664837.

[19] Guy P, Meynaud P, Vincent A, Dudragne G, BaudryG, "Sub-surface damage investigation by high frequency ultrasonic echography on 100Cr6 bearing steel," Tribol. Int., vol. 30, no. 4, pp.247-259, 1997, doi: 10.1016/S0301-679X(96)00041-2.

[20] Murakami Y, "Chapter 1- Mechanism of Fatigue in the Absence of Defects and Inclusions," in Metal Fatigue, 2002, pp.1-10.

[21] Ånmark N, Karasev A, Jönsson P, "The Effect of Different Non-Metallic Inclusions on the Machinability of Steels," Materials (Basel)., vol. 8, no. 2, pp.751-783, Feb. 2015, doi: 10.3390/ma8020751.

[22] Y. MURAKAMI and M. ENDO, "Effects of defects, inclusions and inhomogeneities on fatigue strength," Int. J. Fatigue, vol. 16, no. 3, pp. 163–182, Apr. 1994, doi: 10.1016/0142-1123(94)90001-9.

[23] Frost NE, "A Relation between the Critical Alternating Propagation Stress and Crack Length for Mild Steel," Proc. Inst. Mech. Eng., vol. 173, no. 1, pp.811-836, Jun. 1959, doi: 10.1243/PIME_PROC_1959_173_065_02.

[24] Yukitaka M, Masahiro E, "Quantitative evaluation of fatigue strength of metals containing various small defects or cracks," Eng. Fract. Mech., vol. 17, no. 1, pp.1-15, Jan. 1983, doi: 10.1016/0013-7944(83)90018-8.

[25] Pilkey WD, Pilkey DF, Peterson ' S Stress. 2011.

[26] BSI Standards Publication, "ISO 1143 : 2010 BSI Metallic materials - Rotating bar bending fatigue testing." 2010.

[27] ASTM, "Standard Practice for Conducting Force Controlled Constant Amplitude Axial Fatigue Tests of Metallic Materials," Test, vol. 03, pp.4-8, 2002, doi: 10.1520/E0466-07.2.

[28] "UNI 3964: Mechanical testing of metallic materials - Fatigue testing at room temperature - Genral principles".

[29] Ossola E, Pagliassotto S, Rizzo S, Sesana R, "Microinclusion and Fatigue Performance of Bearing Rolling Elements," pp.321-326, 2019, doi: 10.1007/978-3-030-13980-3_41.

[30] Marin J, Mechanical Behavior of Engineering Materials, Prentice-Hall, Englewood Cliffs, N.J., 1962, p. 224.

[31] Budynas RG, Nisbet JK, Shigley's Mechanical Engineering Design, McGraw Hill, IX ed., 2011, p. 315.